Aloperine inhibits RANKL-induced osteoclast differentiation via suppressing the MAPK signaling pathways

Xiang Wu[1], Caiyun Fu[1], Xuefeng He[1], Shaolei Wang[2]*

[1]Department of Orthopedics, Zhejiang Medical & Health Group Hangzhou Hospital (Hanggang Hospital), Hangzhou, Zhejiang Province, China; [2]Department of Orthopedics, Shaoxing People's Hospital, Shaoxing Hospital of Zhejiang University, Shaoxing, Zhejiang Province, China

***Corresponding Author:** Shaolei Wang, Department of Orthopedics, Shaoxing People's Hospital, Shaoxing Hospital of Zhejiang University, No. 568, Zhongxing North Road, Shaoxing, Zhejiang Province 312000, China. Email: wangshaolei0812@163.com

Received: 29 November 2022; Accepted: 19 December 2022; Published: 31 January 2023

ORIGINAL ARTICLE

Abstract

To figure out the molecular mechanism of aloperine (ALO) on receptor activator of nuclear factor (NF)-kappa-B (κb) ligand (RANKL)-caused osteoclast differentiation. The histopathological analysis and tartrate-resistant acid phosphatase (TRAP) staining assays were applied to check the extent of bone loss of the femur. Then, the protein expressions of nitric oxide synthase 2, glutathione reductase, nuclear erythroid 2-related factor 2, heme oxygenase-1, nicotinamide adenine dinucleotide phosphate (NADPH) oxidase 1, and catalase were checked in RAW264.7, a macrophage cell line, by enzyme-linked-immunosorbent serologic assay and Western blot analysis. Further, the TRAP staining and quantitative polymerase chain reaction assay were applied to characterize the level of RAW264.7 osteoclast differentiation. Besides, Western blot assay was used to check the protein expressions of extracellular regulated protein kinases (ERK), c-Jun N-terminal kinase (JNK), and P38 in RAW264.7. Finally, ERK activation blocker U0126 was used to inhibit mitogen-activated protein kinase (MAPK) signaling pathway to determine the effect of MAPK signaling pathway on RAW264.7 osteoclast differentiation. In this study, the results demonstrated that ALO could inhibit lipopolysaccharide-induced bone loss *in vivo* in a dose-dependent manner, with significant inhibitory effects at high doses. Further research indicated that ALO could inhibit RANKL-induced oxidative stress and osteoclast differentiation of RAW264.7. Then, ALO could inactivate MAPK signaling pathway. Finally, the results showed that inhibition of MAPK signaling pathway could increase ALO inhibition of RANKL-caused osteoclast differentiation. ALO inhibits RANKL-caused osteoclast differentiation by suppressing the MAPK signaling pathways.

Keywords: aloperine (ALO); MAPK; osteoclasts (OCs); RAW264.7

Introduction

Bone diseases are caused by incompatibility between osteoblasts for osteogenesis and osteoclasts (OCs) for resorption-mediated bone remodeling (Feng and McDonald, 2011). Excessive activation of osteoclasts results in excessive destruction of bone, leading to bone diseases caused by bone loss such as osteoporosis, osteolytic metastasis, and rheumatoid arthritis (Hu *et al.*, 2022).

Osteoclasts are the main functional cells for lysing bone matrix and bone resorption. Osteoclasts originate from the mononuclear macrophage system, and play a vital role in bone reconstruction. Macrophage colony stimulating factor (M-CSF) and receptor activator of nuclear

 ISSN 1757-837X online, DOI 10.15586/qas.v15i1.1246

factor (NF)-kappaB (κB) ligand (RANKL are two key cytokines in regulating differentiation and activation of osteoclasts (Charles and Aliprantis, 2014). RANKL can activate NF-κB and mitogen-activated protein kinases (MAPKs, which are extracellular signal-regulated kinases [ERK], Jun N-terminal kinase [JNK], and protein kinase 38 [p38]) by inducing the binding of RANK and tumor necrosis factor (TNF) receptor-associated factor 6 (TRAF6) (Chen *et al*., 2020). These kinases in turn promote the expression of nuclear factor of activated T cells 1 (NFATC1) and c-Fos, the major transcription factor of osteoclast generation, thereby activating the process of osteoclast differentiation (Jang *et al*., 2021).

Aloperine (ALO) is a quinolisidine alkaloid extracted from *Aphorcuroides L.*, and has anti-inflammatory, antiviral, and anti-tumor effects and has been widely used in research fields. ALO can suppress the growth and metastasis of liver cancer, non-small cell lung cancer, ovarian cancer, and other tumors (Liu *et al*., 2019; Muhammad *et al*., 2020; Qiu *et al*., 2020). In terms of anti-inflammation, ALO alleviates dextran sulfate sodium (DSS)-induced colon inflammation in mice by inhibiting PP2A-mediated phosphatidylinositide 3-kinases (PI3K)/protein kinase B (Akt)/mammalian target of rapamycin (mTOR) signal transduction, and proliferation of T cells and lymphocytes (Fu *et al*., 2017).

It has also been reported that ALO suppresses the inflammatory response and oxidative stress of allergic airway in mice and can treat bronchial asthma by inhibiting NF-κB and MAPK pathways and activating the nuclear erythroid 2-related factor 2 (Nrf2)/heme oxygenase-1 (HO-1) pathway (Wang *et al*., 2018). ALO also inhibits the differentiation of cells, such as fibroblasts. ALO protects mice from bleomycin-caused pulmonary fibrosis by inhibiting the proliferation and differentiation of fibroblasts (Yin *et al*., 2018). In addition, ALO also plays crucial roles in the treatment of bone diseases. Research reports have demonstrated that ALO inhibits hypersensitivity reaction and adjuvant arthritis by reducing inflammatory response and oxidative stress (Chang *et al*., 2019). However, the role of ALO in osteoclast differentiation is rarely reported, as the mechanism remains unclear.

In this study, ALO was found to inhibit MAPK pathway activity, thereby inhibiting oxidative stress and osteoclast differentiation of RANKL, thus reducing bone loss.

Materials and Methods

Animals and establishment of bone loss model

A total of 25 Institute of Cancer Research (ICR) mice were obtained from VTrophic Animal Feed High-Tech Co. Ltd. (China). This work was approved by the Ethics Committee of the Hejiang Medical & Health Group Hangzhou Hospital (Hanggang Hospital). All experimental procedures were carried out in accordance with the National Institutes of Health Laboratory Animal Care and Use Guidelines (National Research Council Committee, 2011).

The acquired ICR mice were divided into the following five groups, with five animals in each group (n = 5): Sham, lipopolysaccharide (LPS), LPS + aloperine (ALO; 50 mg/kg), LPS + ALO (100 mg/kg), and LPS + ALO (200 mg/kg). Mice in the LPS-treated groups were injected 5 mg/kg LPS peritoneally to establish a bone loss model. Mice in the ALO-treatment groups were given different doses of ALO orally according to the protocol (Kwak *et al*., 2020).

Histopathological analysis

Samples of the thigh bone were first fixed in 4% (v/v) paraformaldehyde and embedded in paraffin. Next, the thigh bone samples were cut into 3-μm sections and stained with hematoxylin and eosin (H&E) solution (Sigma-Aldrich, St. Louis, MO, USA). Lastly, the pathological samples of the thigh bone were examined under microscope (Zeiss, Germany).

Tartrate-resistant acid phosphatase (TRAP) staining

In order to evaluate the number of osteoclasts, samples of the thigh bone were fixed in 3.85% formalin (Sigma-Aldrich) for 8 min and permeabilized with 0.15% Triton X-100; then, thigh bone samples were treated with TRAP (Sigma-Aldrich). TRAP-positive multinucleated cells were considered as osteoclasts.

Cell culture and establishment of osteoclast genesis model

RAW264.7 was obtained from Beyotime Biotechnology (China). The cells were cultured in Dulbecco's modified eagle *medium* (DMEM; Gibco, USA) with 10% fetal bovine serum (FBS) and 1% penicillin–streptomycin (p/s) in an incubator with 5% CO_2.

In order to generate osteoclasts, RAW264.7 cells (1.5×10^3 cells/well) were separated into five different groups, including control, RANKL, RANKL + ALO (25 μM), RANKL + ALO (50 μM), and RANKL + ALO (100 μM), and cultured for 4 days. Cells in the RANKL treatment groups were treated with 100 ng/mL of RANKL according to the protocol (Zeng *et al*., 2016).

Enzyme-linked-immunosorbent serologic assay (ELISA)

ELISA kits were utilized for detecting nitric oxide synthase 2 (NOS2; ABIN6574224; Biocompare, South

San Francisco, CA, USA) and gutathione reductase (GSR; abx254139; Biocompare) protein levels. The levels of NOS2 and GSR in the supernatant were examined by the corresponding ELISA kits according to manufacturer's instructions.

Western blot analysis

Cells were first washed in phosphate-buffered saline (PBS) for 3 times, and the total proteins was extracted by radioimmunoprecipitation assay (RIPA) buffer (Thermo Fisher Scientific, MA, USA). Total proteins were electrophoresed with sodium dodecyl sulfate–polyacrylamide gel electrophoresis (SDS-PAGE) and transferred to polyvinylidene difluoride (PVDF) membranes. Proteins were identified by specific primary antibodies, including Nrf2 (ab137550, 1:2,500; Abcam, Cambridge, UK), HO-1 (ab213968, 1:3,000; Abcam), NOX1 (ab131088, 1:1000; Abcam), Catalase (ab16731; 1:1,500; Abcam), p-ERK (ab201015; 1:1,500; Abcam), ERK (ab17942; 1:3,000; Abcam), p-JNK (ab4821; 1:1,500; Abcam), JNK (AF1387; 1:3,000; R&D system, Minneapolis, MN, USA), p-P38 (ab4822; 1:1,500; Abcam), P38 (ab170099, 1:2,500; Abcam), and β-actin (ab8227; 1:2,500; Abcam). Then the membranes were incubated with horseradish peroxidase (HRP)-conjugated goat anti-rabbit immunoglobulin G (IgG) secondary antibody (ab205718; 1:1,500; Abcam) and visualized with ECL chemiluminescence reagent (Thermo Fisher Scientific).

Cell Counting Kit-8 (CCK-8) cytotoxicity assay

Cells were seeded in 96-well plates with various concentrations of ALO for different times. Then the CCK-8 solution was added in plates for 2 h and the optical density was tested at 450 nm using a microplate reader (Tecan, Austria).

Quantitative polymerase chain reaction (qPCR)

Trizol reagent (Invitrogen, MA, USA) was applied to isolate total RNAs from cells. Nano Drop 1000 spectrophotometer (Thermo Fisher Scientific) was used to assess the integrity and quantity of isolated RNA. SYBR Premix EX Taq (Takara, Japan) was employed to check the expression of *c-Src* tyrosine kinase (*c-Src*), cathepsin K (*CtSK*), and matrix metalloproteinase-9 (*MMP9*). Primer sequences are shown in Table 1.

Statistical analysis

All data are expressed as mean ± standard error of the mean from three independent experiments. Differences between two groups were compared through Student's *t*-test, and differences between multiple groups were compared through one-way analysis of variance (ANOVA). $P < 0.01$ (two-tailed) was considered statistically significant.

Table 1. Primers for c-Src, CtSK, MMP9, and reference genes.

Genes	Primer	Sequence (5´→3´)
c-Src	Forward	CCAGGCTGAGGAGTGGTACT
	Reverse	CAGCTTGCGGATCTTGTAGT
CtSK	Forward	GGCCAACTCAAGAAGAAAAC
	Reverse	GTGCTTGCTTCCCTTCTGG
MMP9	Forward	AGTTTGGTGTCGCGGAGCAC
	Reverse	TACATGAGCGCTTCCGGCAC
GAPDH	Forward	AACTTTGGCATTGTGGAAGG
	Reverse	ACACATTGGGGGTAGGAACA

GAPDH: glyceraldehyde 3-phosphate dehydrogenase.

Results

Aloperine inhibits lipopolysaccharide-caused bone loss *in vivo*

In order to evaluate the effects of ALO (Figure 1A) on LPS-induced bone loss *in vivo*, the extent of bone loss of the femur was assessed by administering different doses of ALO with or without LPS. The H&E staining result revealed that the inflammatory osteolysis and trabecular bone loss were increased in the LPS-treated group, while bone matrix was gradually restored in the LPS-induced group treated with an increased dose of ALO (Figures 1B and 1C). The TRAP staining of the femur also suggested the protective effect of ALO on LPS-induced trabecular bone loss. The pink area of TRAP staining represents osteoclasts. The number of osteoclasts per field was dramatically higher in the LPS group, while their number per field was gradually decreased when LPS-induced mice was treated with ALO (Figures 1D and 1E). These results suggested that ALO could inhibit LPS-induced bone loss *in vivo*.

Aloperine inhibits RANKL-caused oxidative stress of RAW264.7

In order to determine the effects of ALO on RANKL-caused oxidative stress of mouse macrophage cell line, RAW264.7, the expressions of oxidative stress-related proteins were assessed. RAW264.7 cells were exposed to different concentrations of ALO with or without RANKL; the protein expressions of nitric oxide synthase 2 (NOS2), glutathione reductase (GSR), Nrf2, HO-1, nicotinamide

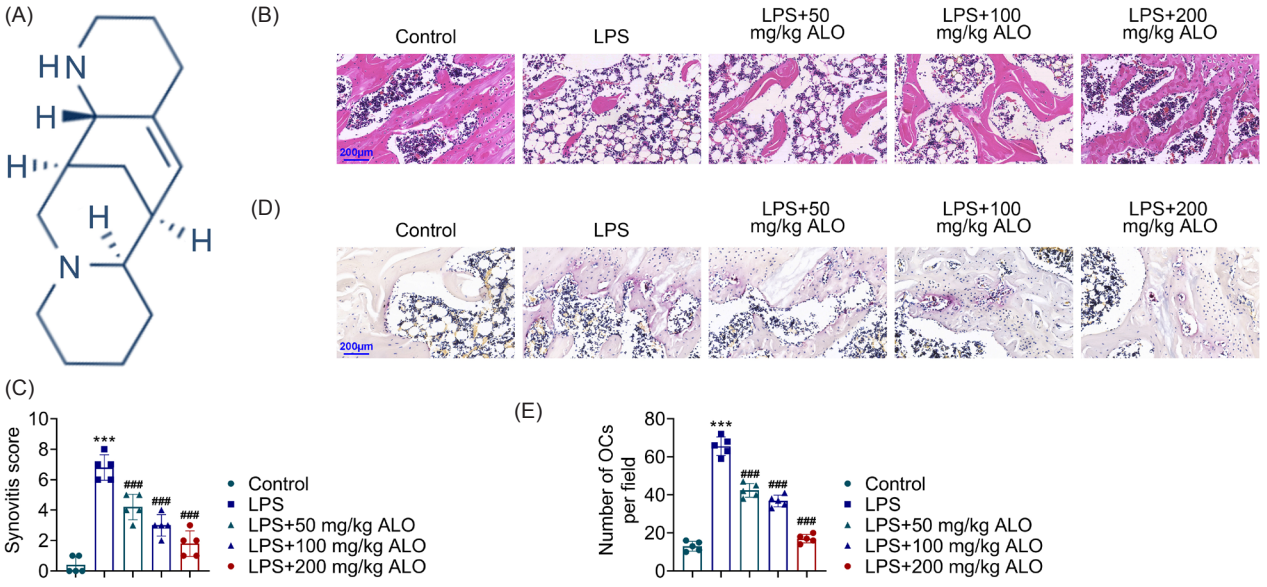

Figure 1. Aloperine inhibits LPS-induced bone loss *in vivo*. (A) Chemical formula of ALO. (B) H&E staining of the femur in each group. (C) TRAP staining of the femur in each group. Data were presented as mean ± SD with three independent experiments.

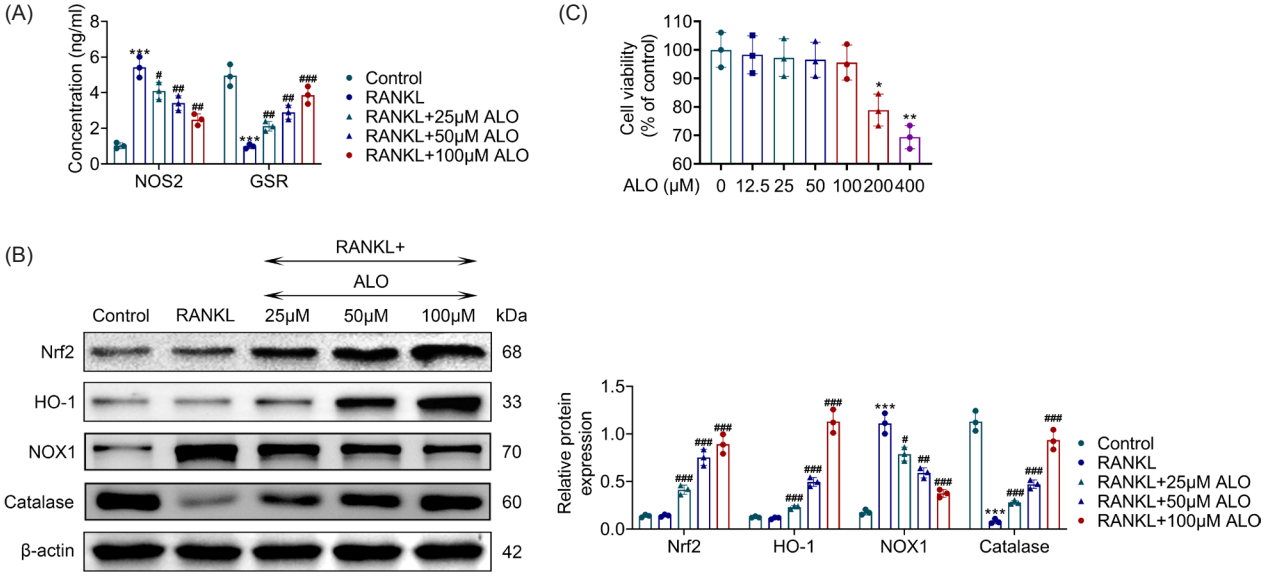

Figure 2. Aloperine inhibits RANKL-induced oxidative stress of RAW264.7. (A) Protein expressions of NOS2 and GSR in RAW264.7 in each group. (B) Protein expressions of Nrf2, HO-1, NOX1, and catalase in RAW264.7 in each group. (C) The cell viability of RAW264.7 was checked by CCK8. Data were presented as mean ± S.D. with three independent experiments. ***P < 0.001 versus the control group, #P < 0.05, ##P < 0.01, and ###P < 0.001 versus the RANKL-treated group.

adenine dinucleotide phosphate (NADPH) oxidase 1 (NOX1), and catalase in RAW264.7 cell line were determined by ELISA and Western blot analysis. Results of ELISA and Western blot analysis proved that RANKL treatment increased the protein expressions of NOS2 and NOX1, and these two nitric oxide and superoxide producers enhanced the level of reactive oxidative species (ROS) (Figure 2A).

In addition, the RANKL treatment decreased the protein expressions of GSR, Nrf2, HO-1, and catalase, and these important transcription factors, which regulate the oxidative stress response of cells, can reduce ROS level (Figure 2B). However, proteins that were increased or decreased by RANKL treatment were reversed by different concentrations of ALO, obviously with reversal effects at high doses (Figures 2A and 2B). In order

to exclude the possibility that ALO inhibits RANKL-induced oxidative stress of RAW264.7 by cytotoxicity, RAW264.7 cells were subjected to cytotoxicity experiments (Figure 2C). We found that ALO had no cytotoxic effect on osteoclast precursor cells. These results hinted that ALO could inhibit RANKL-caused oxidative stress of RAW264.7.

Aloperine inhibits RANKL-caused osteoclast differentiation of RAW264.7

We next investigated the effects of ALO on RANKL-caused osteoclast differentiation of RAW264.7. TRAP staining was applied to estimate the number of osteoclasts to characterize the level of RAW264.7 osteoclast differentiation. Besides, expressions of *c-Src*, *CtSK*, and *MMP9* were also measured by qPCR assay to examine the RAW264.7 osteoclast differentiation. Both TRAP staining and qPCR results confirmed that RANKL caused osteoclast differentiation of RAW264.7, while ALO inhibited RANKL-caused osteoclast differentiation, and as the concentration of ALO increased, the effect of inhibiting RANKL-caused osteoclast differentiation became more obvious (Figures 3A and 3B). These results declared that ALO inhibited the RANKL-caused osteoclast differentiation of RAW264.7

Aloperine inhibits the MAPK signaling pathway

In order to estimate the mechanism of ALO on inhibition of RANKL-induced osteoclast differentiation via suppressing the MAPK signaling pathways, Western blot analysis was applied to check the expression of ERK, JNK, and P38 in RAW264.7. The Western blot results demonstrated that the phosphorylation of ERK, JNK, and P38 showed a dramatic upregulation in RAW264.7 after RANKL treatment. However, the phosphorylation of ERK, JNK, and P38 were reversed in RANKL group administrated with ALO, indicating that ALO inactivated MAPK signaling pathway. Subsequently, we used ERK activator blocker U0126 to inhibit MAPK signaling. The results showed that U0126 also significantly reversed the phosphorylation of ERK, JNK, and P38 (Figure 4). These results suggested that ALO inhibited RANKL-caused osteoclast differentiation by suppressing MAPK pathways.

Inhibition of MAPK signaling pathway increases aloperine inhibition of RANKL-caused osteoclast differentiation

Furthermore, to determine the effects of ALO and MAPK signaling pathway on RANKL-caused osteoclast differentiation of RAW264.7, TRAP staining was applied to estimate the number of osteoclasts to characterize the level of RAW264.7 osteoclast differentiation. Besides, the expressions of *c-Src*, *CtSK*, and *MMP9* were also measured by qPCR assay to determine the level of RAW264.7 osteoclast differentiation. As expected, both TRAP staining and qPCR results confirmed that RANKL caused osteoclast differentiation of RAW264.7, while ALO inhibited RANKL-caused osteoclast differentiation. To determine the involvement of MAPK signaling pathway in mediating the inhibitory effect of ALO on RANKL-induced osteoclast differentiation, ERK activation blocker U0126 was used to inhibit MAPK signaling pathway. The TRAP staining and qPCR results showed that inhibition of MAPK signaling pathway increased the ALO inhibition of RANKL-caused osteoclast differentiation (Figure 5A and 5B). Further inhibition of osteoclast formation was found through the combined use of ALO

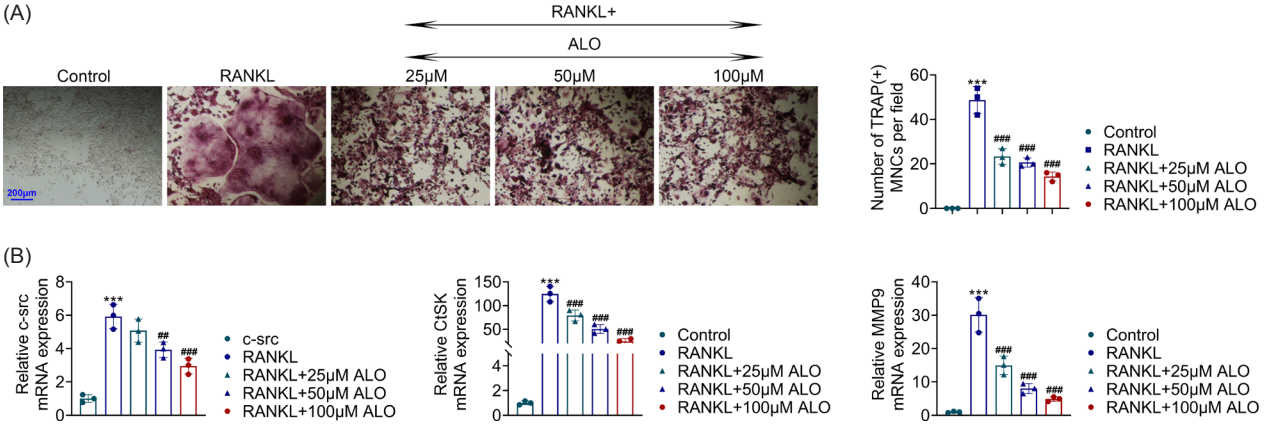

Figure 3. Aloperine inhibits RANKL-induced osteoclast differentiation of RAW264.7 cells. (A) TRAP staining of RAW264.7. (B) mRNA expressions of *c-Src*, *CtSK*, and *MMP9* in RAW264.7. Data were presented as mean ± S.D. with three independent experiments. ***P < 0.001 versus the control group and $^{###}$P < 0.001 versus the RANKL-treated group.

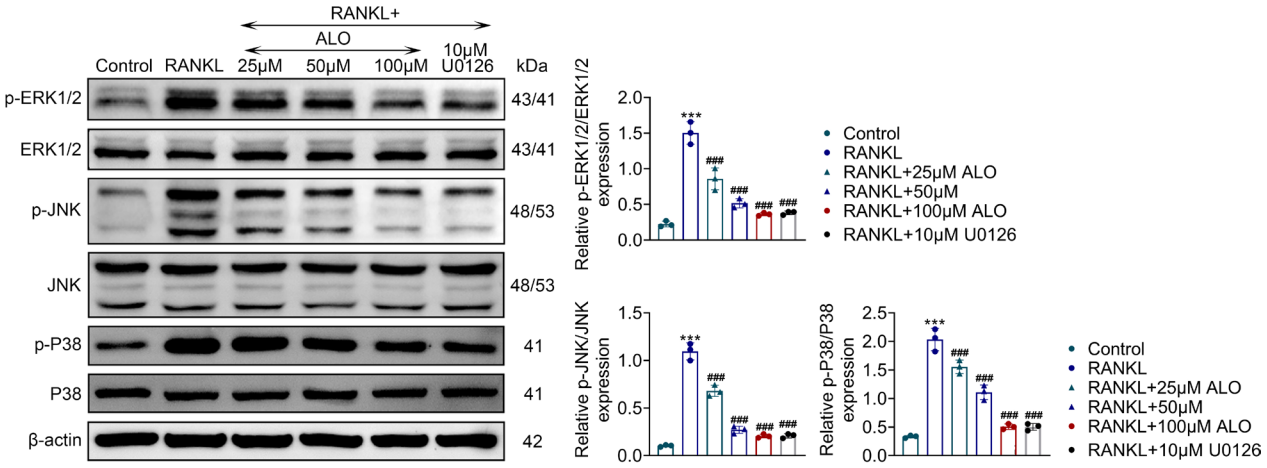

Figure 4. Aloperine inhibits MAPK signaling pathway. Protein expressions of ERK, JNK, and P38 in RAW264.7 cells. Data were presented as mean ± SD with three independent experiments. ***P < 0.001 versus the control group, ##P < 0.01, and ###P < 0.001 versus the RANKL-treated group.

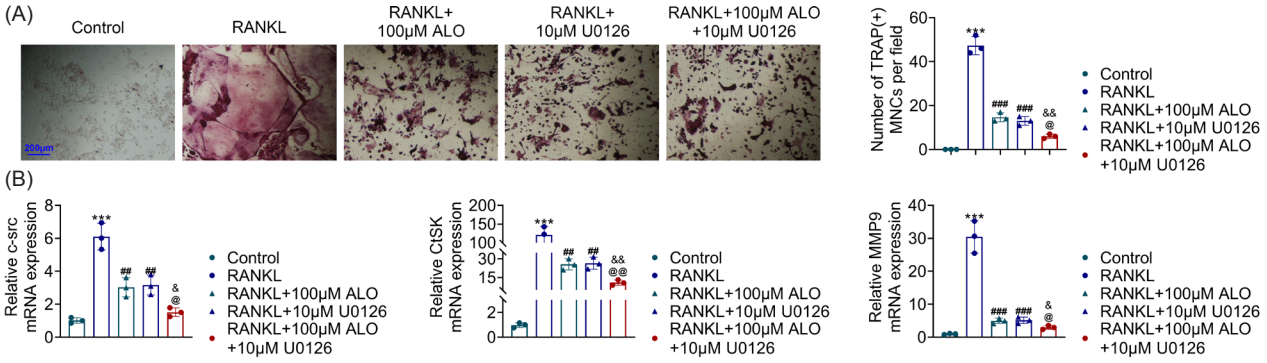

Figure 5. Inhibition of MAPK signaling pathway increases the ALO inhibition of RANKL-induced osteoclast differentiation. (A) TRAP staining of RAW264.7 cells. (B) mRNA expressions of *c-Src*, *CtSK*, and *MMP9* in RAW264.7. Data were presented as mean ± SD with three independent experiments. ***P < 0.001 versus the control group, ##P < 0.01, ###P < 0.001 versus the RANKL-treated group, &P < 0.05, &&P < 0.01 versus RANKL + 100-uM ALO-treated group, @P < 0.05 and @@P < 0.01 versus RANKL + 10-uM U0126-treated group.

and ERK inhibitors, which further demonstrated the necessity and influence of ERK signaling pathway on formation of osteoclasts.

Discussion

Although the clinical research on bone diseases has developed, the molecular mechanism of bone diseases is not clear. Recently, ALO has been shown to have the potential to play a vital role in anti-inflammatory, antiviral, and anti-tumor aspects (Huang *et al.*, 2021). However, there are few studies on functioning of ALO in bone diseases, and studying the molecular regulation mechanism of ALO in bone diseases may offer new therapeutic targets for these diseases.

Aloperine is a quinolisidine alkaloid extracted from *Aphorcuroides L.*, which has been widely used in varied research fields, such as inflammation, hypertension, and vasodilation (Li *et al.*, 2020; Zhong *et al.*, 2020). ALO has also been reported to markedly diminish the clinical manifestations of Alzheimer's disease (Zhao *et al.*, 2018), cardiovascular disease (Huang *et al.*, 2020), and other diseases. Specifically, ALO exerts antitumor effects on cancer of the bladder (Zhang *et al.*, 2022). Recently, the relationship between ALO and vasodilatory effects in rat aorta has been confirmed (Yang *et al.*, 2018). Moreover, ALO has been found to have anti-liver fibrogenic effect (Wang *et al.*, 2020). As a promising natural product, ALO has prospects in the development of safe new drugs because of multi-target actions. However, there are few studies on the pharmacological effects

of ALO on bone diseases, and its possible mechanism has not been reported. This study established that ALO inhibits LPS-induced bone loss *in vivo*. In addition, it is also confirmed that ALO inhibits RANKL-caused oxidative stress of RAW264.7. Furthermore, ALO suppresses RANKL-caused osteoclast differentiation of RAW264.7. These results confirm that ALO improves clinical manifestations of bone diseases and RANKL-caused osteoclast differentiation.

An increasing number of research studies have established that ALO performed their functions by mediating the expressions of target *messenger RNAs* (mRNAs). Studies revealed that ALO could reverse cisplatin resistance in colorectal cancer cells by inhibiting HIF-1α/ERK pathway (Zheng *et al*., 2020). Moreover, ALO was reported to protect human epithelial cells against oxidative stress and apoptosis via regulating Nrf2/HO-1 signaling pathway (Zhang *et al*., 2020). In addition, ALO protected myocardial injury in rats via activation the PI3K/Akt pathway (Mao *et al*., 2019). Another discovery in this study was that ERK, JNK, and P38 proteins are the targets of ALO. Activated ERK is involved in cell proliferation, differentiation, and cytoskeleton construction. NF-κB participates in cellular response to various stimuli. Here, it was confirmed that ALO could act on ERK, JNK, and P38. Changes in ERK, JNK, and P38 protein expressions caused by RANKL were gradually changed by increasing ALO dose, suggesting that ALO improved clinical manifestations of osteoclast differentiation by inactivating MAPK.

Conclusion

Our results establish that ALO inhibits LPS-induced bone loss *in vivo*. Moreover, ALO inhibits RANKL-caused oxidative stress of RAW264.7. Meanwhile, ALO suppresses RANKL-caused osteoclast differentiation of RAW264.7. Furthermore, the fact that ALO improves clinical manifestations of osteoclast differentiation by inactivating MAPK pathway is also confirmed. Finally, ERK activation blocker U0126 was used to inhibit MAPK signaling pathway and the result showed that inhibition of MAPK signaling pathway could increase ALO inhibition on RANKL-induced osteoclast. All these results revealed the role of ALO/ERK/JUK/NF-κB in improving clinical manifestations of osteoclast differentiation, which could substantially lay a solid foundation for further treatment of bone diseases.

Conflict of interest

The authors state that there were no conflicts of interest to disclose.

Author Contributions

Xiang Wu and Caiyun Fu designed the study, supervised the data collection, and analyzed and interpreted the data. Xuefeng He and Shaolei Wang prepared and reviewed the draft of the manuscript for publication. All authors read and approved the final manuscript.

Data Availability Statement

The data that support the findings of this study are available from the corresponding author upon reasonable request.

References

Charles J.F. and Aliprantis A.O. 2014. Osteoclasts: more than "bone eaters." *Trends* in *Molecular Medicine* 20(8): 449–459. https://doi.org/10.1016/j.molmed.2014.06.001. PMID: 25008556.

Chang Z., Zhang P., Zhang M., Jun F., Hu Z., Yang J., Wu Y. and Zhou R. 2019. Aloperine suppresses human pulmonary vascular smooth muscle cell proliferation via inhibiting inflammatory response. Chinese Journal of Physiology 62(4): 157–165. https://doi.org/10.4103/cjp.Cjp_27_19. PMID: 31535631.

Chen H., Fang C., Zhi X., Song S., Gu Y., Chen X., Cui J., Hu Y., Weng W., Zhou Q., Wang Y., Wang Y., Jiang H., Li X., Cao L., Chen X., Su J. 2020. Neobavaisoflavone inhibits osteoclastogenesis through blocking RANKL signalling-mediated TRAF6 and c-Src recruitment and NF-κB, MAPK and Akt pathways. Journal of Cellular and Molecular Medicine 24(16): 9067–9084. https://doi.org/10.1111/jcmm.15543. PMID: 32604472.

Feng X. and McDonald J.M. 2011. Disorders of bone remodeling. Annual Review of Pathology 6: 121–145. https://doi.org/10.1146/annurev-pathol-011110-130203. PMID: 20936937.

Fu X., Sun F., Wang F., Zhang J., Zheng B., Zhong J., Yue T., Zheng X., Xu J.F. and Wang C.Y. 2017. Aloperine protects mice against DSS-induced colitis by PP2A-mediated PI3K/Akt/mTOR signaling suppression. *Mediators* of *Inflammation* 2017: 5706152. https://doi.org/10.1155/2017/5706152. PMID: 29056830.

Hu L., Liu R. and Zhang L. 2022. Advance in bone destruction participated by JAK/STAT in rheumatoid arthritis and therapeutic effect of JAK/STAT inhibitors. *International Immunopharmacology* 111: 109095. https://doi.org/10.1016/j.intimp.2022.109095. PMID: 35926270.

Huang B., Xiong J., Zhao X., Zheng Y. and Zhu N. 2020. Network pharmacology-based analysis of the pharmacological mechanisms of aloperine on cardiovascular disease. Evidence-Based Complementary and Alternative Medicine 2020: 5180716. https://doi.org/10.1155/2020/5180716. PMID: 32733582.

Huang S., Zhang Y., Zhang Y., Liu J., Liu Z. and Wang X. 2021. Establishment of LC-MS/MS method for determination of aloperine in rat plasma and its application in preclinical pharmacokinetics. *Journal of Chromatography B: Analytical* Technologies in the *Biomedical* and *Life Sciences* 1173: 122671. https://doi.org/10.1016/j.jchromb.2021.122671. PMID: 33819795.

Jang H.Y., Lee H.S., Noh E.M., Kim J.M., You Y.O., Lee G., Koo J.H., Lim H., Ko S., Kim J.S., Lee J.H., Lee Y.R. 2021. Aqueous extract of Chrysanthemum morifolium Ramat. inhibits RANKL-induced osteoclast differentiation by suppressing the c-fos/NFATc1 pathway. Archives of Oral Biology 122: 105029. https://doi.org/10.1016/j.archoralbio.2020.105029. PMID: 33387850.

Kwak S.C., Cheon Y.H., Lee C.H., Jun H.Y., Yoon K.H., Lee M.S., and Kim J.Y. 2020. Grape seed proanthocyanidin extract prevents bone loss via regulation of osteoclast differentiation, apoptosis, and proliferation. Nutrients 12(10): 3164. https://doi.org/10.3390/nu12103164. PMID: 33081167.

Li W., Li Y., Zhao Y. and Ren L. 2020. The protective effects of aloperine against ox-LDL-induced endothelial dysfunction and inflammation in HUVECs. Artificial Cells, Nanomedicine, and Biotechnology 48(1): 107–115. https://doi.org/10.1080/21691401.2019.1699816. PMID: 31852304.

Liu J.S., Huo C.Y., Cao H.H., Fan C.L., Hu J.Y., Deng L.J., Lu Z.B., Yang H.Y., Yu L.Z., Mo Z.X., Yu Z.L. 2019. Aloperine induces apoptosis and G2/M cell cycle arrest in hepatocellular carcinoma cells through the PI3K/Akt signaling pathway. Phytomedicine 61: 152843. https://doi.org/10.1016/j.phymed.2019.152843. PMID: 31039533.

Mao Q., Guo F., Liang X., Wu Y. and Lu Y. 2019. Aloperine activates the PI3K/Akt pathway and protects against coronary microembolisation-induced myocardial injury in rats. Pharmacology 104(1–2): 90–97. https://doi.org/10.1159/000500761. PMID: 31163448.

Muhammad T., Sakhawat A., Khan A.A., Huang H., Khan H.R., Huang Y. and Wang J. 2020. Aloperine in combination with therapeutic adenoviral vector synergistically suppressed the growth of non-small cell lung cancer. Journal of Cancer Research and Clinical Oncology 146(4): 861–874. https://doi.org/10.1007/s00432-020-03157-2. PMID: 32088783.

National Research Council (US) Committee for the Update of the Guide for the Care and Use of Laboratory Animals. 2011. Guide for the care and use of laboratory animals. 8th ed. Washington, DC: National Academy of Sciences, National Academies Press (US). Reports funded by National Institutes of Health. PMID: 21595115.

Qiu M., Liu J., Su Y., Liu J., Wu C. and Zhao B. 2020. Aloperine induces apoptosis by a reactive oxygen species activation mechanism in human ovarian cancer cells. *Protein & Peptide Letters* 27(9): 860–869. https://doi.org/10.2174/0929866527666200320094313. PMID: 32196436.

Wang C., Choi Y.H., Xian Z., Zheng M., Piao H. and Yan G. 2018. Aloperine suppresses allergic airway inflammation through NF-κB, MAPK, and Nrf2/HO-1 signaling pathways in mice. *International Immunopharmacology* 65: 571–579. https://doi.org/10.1016/j.intimp.2018.11.003. PMID: 30415164.

Wang K., Guo Z., Bao Y., Pang Y., Li Y., He H. and Song D. 2020. Structure–activity relationship of aloperine derivatives as new anti-liver fibrogenic agents. Molecules 25(21): 4977. https://doi.org/10.3390/molecules25214977. PMID: 33121156.

Yang C., Yu Y., Wu F., Wu Y., Feng J., Yan L., Han L., Ren J., Nie L. and Zhou R. 2018. Vasodilatory effects of aloperine in rat aorta and its possible mechanisms. Chinese Journal of Physiology 61(5): 293–301. https://doi.org/10.4077/cjp.2018.Bah609. PMID: 30384550.

Yin W., Han J., Zhang Z., Han Z. and Wang S. 2018. Aloperine protects mice against bleomycin-induced pulmonary fibrosis by attenuating fibroblast proliferation and differentiation. Scientific Reports 8(1): 6265. https://doi.org/10.1038/s41598-018-24565-y. PMID: 29674691.

Zeng X-z., He L-g., Wang S., Wang K., Zhang Y-y., Tao L., Li X-j. and Liu S-w. 2016. Aconine inhibits RANKL-induced osteoclast differentiation in RAW264.7 cells by suppressing NF-κB and NFATc1 activation and DC-STAMP expression. *Acta Pharmacologica Sinica* 37(2): 255–263. https://doi.org/10.1038/aps.2015.85. PMID: 26592521.

Zhang L., Liang J., Liu X., Wu J., Tan D. and Hu W. 2020. Aloperine exerts antitumor effects on bladder cancer *in vitro*. Onco Targets and Therapy 13: 10351–10360. https://doi.org/10.2147/ott.S260215. PMID: 33116615.

Zhang J., Zhou H., Chen J., Lv X. and Liu H. 2022. Aloperine protects human retinal pigment epithelial cells against hydrogen peroxide-induced oxidative stress and apoptosis through activation of Nrf2/HO-1 pathway. *Journal* of Receptors and *Signal Transduction* 42(1): 88–94. https://doi.org/10.1080/10799893.2020.1850787. PMID: 33256538.

Zhao J., Zhang G., Li M., Luo Q., Leng Y. and Liu X. 2018. Neuroprotective effects of aloperine in an Alzheimer's disease cellular model. Biomedicine & Pharmacotherapy 108: 137–143. https://doi.org/10.1016/j.biopha.2018.09.008. PMID: 30218858.

Zheng H., Zhang A., Li D., Ke X., Wang Q., Yan S., Xue Y. and Deng X. 2020. Aloperine can reverse the cisplatin resistance of colorectal cancer cells via suppressing the HIF-1α/ERK signaling pathway. Pharmazie. 75(11): 581–585. https://doi.org/10.1691/ph.2020.0672. PMID: 33239133.

Zhong H., Hao L., Li X., Wang C. and Wu X. 2020. Anti-inflammatory role of trilobatin on lipopolysaccharide-induced acute lung injury through activation of AMPK/GSK3β-Nrf2 pathway. Signa Vitae. 6(2): 160–166. https://doi.org/10.22514/sv.2020.16.0075. PMID: 26592521.